Scale Model of an Ink Jet

Abstract: A scale model, approximately fifty times the size of its prototype, was used to study drop formation of an ink jet. Viscosity, surface tension, and inertial forces were modeled; gravity and air drag forces were not. The model accurately predicted operating conditions leading to the formation of undesirable satellite drops, thus permitting evaluation of measures designed to avoid them.

Introduction

After a cylindrical liquid jet emerges from a nozzle, it tends to form drops at some distance from the nozzle. This decay of the jet is caused by an instability created by the existence of surface tension. Certain infinitesimal disturbances of the jet thus grow until drops are formed. These disturbances (e.g., noise, vibration, liquid inhomogeneity) tend to be random. As a consequence, the drop formation frequency and the distance from the nozzle where drops first occur vary randomly. Such a process is unsuitable for a printer in which each drop formed is individually addressed to assure that it will reach the proper point on the page being printed.

The formation of drops can be forced to occur at a well-defined frequency and distance from the nozzle by perturbing the jet periodically with sufficient strength so that random environmental disturbances have a negligible effect. This possibility was known at least as early as 1833 by Savart [1]. In 1859 Magnus reported a systematic experimental investigation of stream breakup [2], including visualization of drops by stroboscopic techniques. Given a certain jet velocity and diameter, it was found (both analytically and experimentally) that certain disturbance frequencies caused drops to appear closer to the nozzle than other frequencies [3]. One method of exciting the jet to cause periodic drop formation is to introduce a periodic pressure variation at the pressure side of the nozzle [4].

Under most operating conditions in which a jet decays into drops, more than one drop is formed for every period of the exciting signal. Of the several drops formed, one is usually significantly larger than the others; this is the drop desired for printing. The others, called satellites, detrimentally affect the printing process by disturbing desired drop charging [5] or by impacting the print-

ed page in undesired locations. It is therefore crucial to avoid forming these satellite drops in a high quality printer.

A number of analyses exist of the capillary (i.e., surface tension induced) breakup of a liquid jet. Linear analyses [3, 6, 7] generally predict reasonable values for the exponential growth rate of drop-forming disturbances; however, because of the assumptions involved, they do not generate information about the occurrence of satellites. Satellites are predicted by nonlinear analyses [7-9]. However, even these are inadequate for obtaining operationally useful predictions of satellite-free conditions. At this time no analysis has been published that satisfactorily explains satellite formation as a function of driving signal waveform, amplitude, exact nozzle shape, and fluid properties. Among the published experimental investigations [9-11], we found none that covered all the characteristics important to us in designing an ink jet printer; however, [16] establishes a useful correlation between drop spacing, breakup time, and satellite occurrence for sinusoidal excitation.

Because of the small size of a printer jet (less than 40 μ m) and the high frequency of drop formation (higher than 100 kHz), two phases in the development of acceptably performing hardware were particularly difficult. One relates to manufacturing nozzles satisfying stringent requirements of diameter, length, entrance and exit edge condition, and freedom from burrs and imperfections. The other involves the visual detection of satellites under all printer operating conditions. A scale model (approximately fifty times prototype size) to simulate those aspects of jet dynamics thought to be most important was designed, built, and operated so as to better understand satellite formation under conditions more easily

controlled and observed. The model simulates those aspects of drop formation involving the nozzle, the shape and amplitude of the pressure disturbance upstream from the nozzle, fluid properties, and drop formation frequency. Operation of the printer "head" assembly, involving vibration of a piezoelectric crystal diaphragm and transmission of this disturbance from the diaphragm through the liquid to the entrance of the nozzle, was not simulated.

In this paper we describe the use of the scale model to study the drop formation characteristics of an ink jet printer nozzle. Also described is a dimensional analysis of the system parameters and variables judged to be significant and the useful set of dimensionless parameters obtained. These parameters include modified Reynolds and Weber numbers that proved to be particularly valuable when evaluating drop formation by means of a "velocity print window" plot. (The print window is an area in the plane formed by the disturbance amplitude and the axial drop spacing axes in which printing is possible because satellites are absent.) The considerations that led to a choice of the model liquid – a mixture of water and glycerol-are presented with a description of the modeling apparatus. Several tests are described that were used to determine if the behavior of the scale model accurately represented that of the prototype. The second half of the paper deals with the results of the investigation; it discusses the influence of various parameters, such as temperature, orifice geometry, and fluid properties on the print window.

Dimensional analysis

The theory of similitude asserts that two physical systems may exhibit behavior such that the variables measured on one may be directly related to the variables measured on the other, even though the parameters describing the two, such as length, viscosity, or surface tension, may be quite different in magnitude [12]. Of the two systems discussed in this paper the one designated the prototype was the system we needed to understand; the other, the model, was designed and operated so that its behavior could be directly related to that of the prototype.

Great difficulty was encountered during the development of an ink jet printer, both in controlling parameters affecting drop formation (e.g., orifice diameter, length, and exact geometry) and in observing the details of the drop formation process. The desired ink stream was typically 25.4 to 38.1 μ m (0.001 to 0.0015 in.) in diameter, and drops were formed at rates between 100 kHz and 120 kHz. Figure 1 depicts the jet breakup and identifies the significant parameters and variables. Symbols \tilde{p} and \tilde{v} designate the average values of pressure and stream velocity, respectively, and \tilde{p} and \tilde{v} are perameters and \tilde{v} are per-

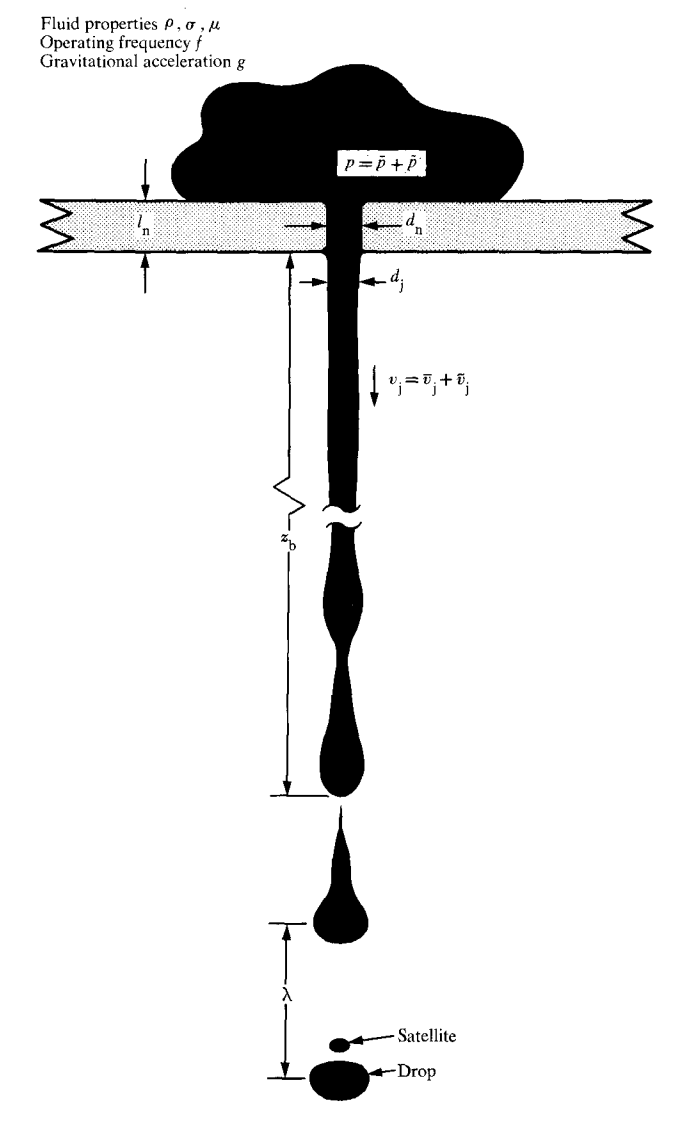


Figure 1 Ink jet breakup.

turbations of these quantities varying in a periodic manner at the drop generation frequency. The effect of the air surrounding the jet is ignored. The symbols shown are those associated with the prototype. (A glossary is provided in the Appendix.) Model symbols are identified by adding an asterisk (e.g., \bar{p}^*) to the prototype symbol. From this set of parameters and variables an infinite number of sets of dimensionless parameters could be constructed; however, the set shown in Table 1 was considered to be the most useful.

Dimensionless parameters \underline{We} , \underline{Re} , and \underline{Fr} are Weber, Reynolds, and Froude numbers modified by the factors $(\lambda/d_n)^{-2}$, $(\lambda/d_n)^{-1}$, and $(\lambda/d_n)^{-1}$, respectively. These modified dimensionless parameters were found to be convenient for this investigation because their values are

Table 1 Dimensionless parameters.

Modified Weber number	$\underline{We} = \frac{\rho \bar{v}_{j}^{2} d_{n}}{\sigma} \left(\frac{\lambda}{d_{n}}\right)^{-2} = \frac{\rho f^{2} d_{n}^{\beta}}{\sigma}$
Modified Reynolds number	$\underline{Re} = \frac{\rho \bar{v}_{j} d_{n}}{\mu} \left(\frac{\lambda}{d_{n}}\right)^{-1} = \frac{\rho f d_{n}^{2}}{\mu}$
Modified Froude number	$\underline{Fr} = \sqrt{\frac{\bar{v}_{i}^{2}}{gd_{n}}} \left(\frac{\lambda}{d_{n}}\right)^{-1} = f\sqrt{\frac{d_{n}}{g}}$
Modified Strouhal number	$\underline{St} = 1 = \frac{\bar{v}_{j}}{fd_{n}} \left(\frac{\lambda}{d_{n}}\right)^{-1} = \frac{\bar{v}_{j}}{f\lambda}$
Pressure coefficient	$c_{\rm p} = \frac{\bar{p}}{\rho \bar{v}_{\rm i}^2}$
Velocity ratio	$\mathbf{\Omega}_{\mathrm{v_{j}}} = \frac{\tilde{v}_{\mathrm{j}}}{\tilde{v}_{\mathrm{j}}}$
Pressure ratio	$\Omega_{ m p}=rac{ ilde{p}}{ ilde{p}}$
Nozzle aspect ratio	$\Gamma_1 = \frac{l_n}{d_n}$
Dimensionless wavelength	$\Gamma_{\lambda} = \frac{\lambda}{d_{\rm n}}$
Nozzle contraction coefficient	$\Gamma_{\rm d} = \frac{d_{\rm j}}{d_{\rm n}}$
Dimensionless breakup distance	$\Gamma_z = \frac{z_{ m b}}{\lambda}$
Satellite number	$\Gamma_{\rm s}=$ any other geometrical ratio that describes the stream or satellite configuration

independent of stream velocity \bar{v} and drop spacing λ and thus are constant for all data used to plot one print window. The modified Strouhal number \underline{St} equals unity by definition and is used to determine \bar{v} from measurements of f and λ .

Some of the dimensionless parameters (We, Re, Fr, Γ_1 , Γ_2) can be considered "input" parameters because they are controlled by the experimenter. Others (c_p, Γ_d) Γ_z , Ω_{v_s} , Ω_{p_s} , Γ_s) can be considered "output" parameters because they are observed as functions of the inputs. Ideally, the model would be designed to duplicate all input parameters. However, we were unable to find a model liquid that would have allowed us to satisfy all input parameters and still have a worthwhile scale-up of about 50X. The difficulty was not in modeling Re but in modeling both We and Fr. Since breakup depends primarily on the interaction between surface tension and liquid inertia, it was important to keep the modified Weber number. The modified Froude number, which relates to the effects of gravity, was thus ignored. Indeed, the behavior of the model differed from the prototype; because of gravity, drop-to-drop spacing in the

model increased with distance from the nozzle much more than in the prototype. Fortunately, the modeling of satellite formation was apparently not seriously affected.

The desire to have the model duplicate prototype performance while ignoring gravitational effects amounts to requiring that the model input parameters $\underline{W}e^*$, $\underline{R}e^*$, Γ_1^* , and Γ_{λ}^* equal the corresponding prototype parameters. These four model parameters contain seven unknowns $(\rho^*, f^*, d_n^*, \sigma^*, \mu^*, l_n^*, \lambda^*)$. One can thus introduce three more arbitrary definitions; for convenience the following were chosen:

$$K = \frac{d_n^*}{d_n} = \frac{l_n^*}{l_n} = \frac{\lambda^*}{\lambda},$$

$$R = \frac{\rho^*}{\rho},$$

$$S = \frac{\sigma^*}{\sigma}.$$

Note here that K is the geometrical scale factor. Based on these ratios, one finds

$$\frac{f^*}{f} = \left(\frac{S}{RK^3}\right)^{\frac{1}{2}},\tag{1}$$

$$\frac{\mu^*}{\mu} = (KRS)^{\frac{1}{2}}. (2)$$

Model fluid

To properly model the ink, its properties had to be known. Both ρ and μ are easily measured; however, the choice of a value for σ was not obvious because the ink is a water-surfactant mixture that is known to develop its final surface tension over a relatively long period of time as the surfactant migrates to the surface [13]. It is generally assumed that a new surface has the surface tension of the solvent and that it then decreases to its static value. Since drop formation in the prototype occurs in less than 100 μ s, we assumed that during this time the ink had the surface tension of water (72.5 mN/m). Linear drop formation theories predict that the slope of the linear portion of the curves shown in Fig. 2 should be inversely proportional to the square root of surface tension [3]. The similarity of the slopes of the curves for both the prototype and the model justified the choice of the surface tension of water as the dynamic surface tension of the ink.

Among the three fluid parameters of interest $(\rho^*, \sigma^*, \mu^*)$, the first two are not controllable over wide ranges once a particular class of fluids is chosen. (This is the reason for choosing ratios R and S rather than some other conditions.) Viscosity μ^* , however, can usually be easily varied by, for example, heating or varying the relative concentrations of components making up the liquid. Once a scale factor and a class of fluids is chosen,

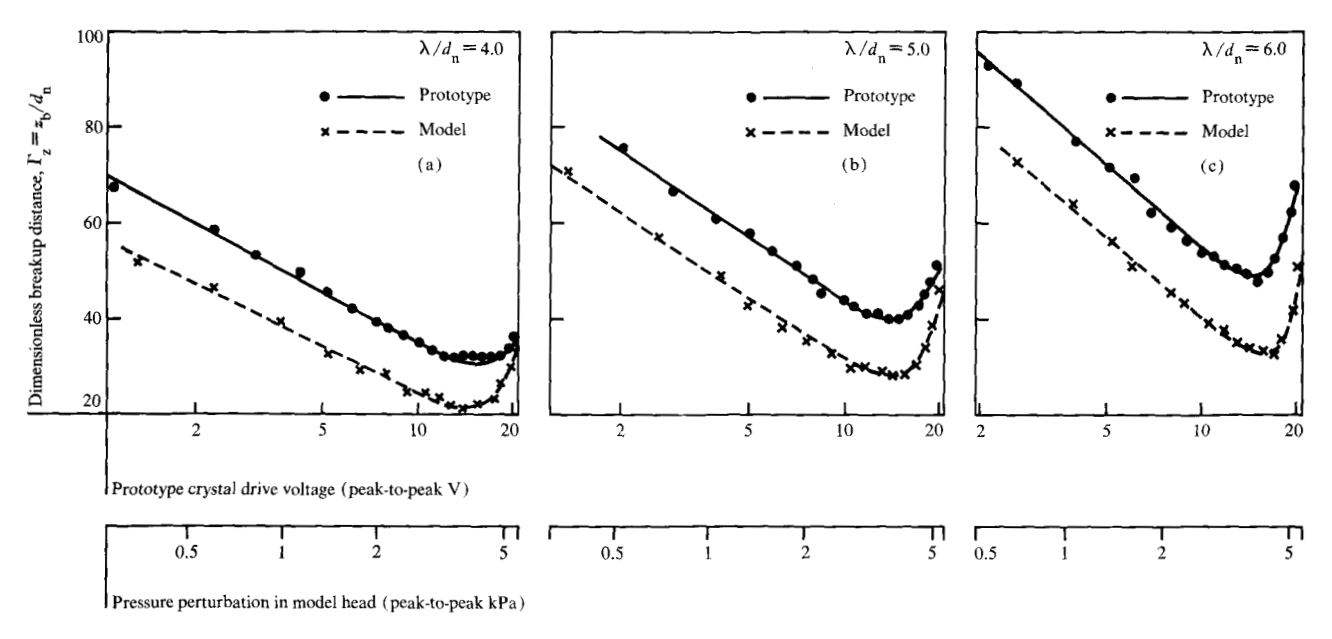


Figure 2 Breakup length as a function of disturbance amplitude.

parameter K is known and parameters R and S are known to be within a narrow range. Equations (1) and (2) were then used to compute the drop formation frequency and the needed viscosity of the model fluid.

A number of fluid systems were considered for model use, among them an aqueous sucrose solution and mineral oils. The fluid finally chosen was a mixture of water and glycerol (approximately 30:70 by weight); to this was added 4 percent by weight of a nontoxic and nonsurfactant organic salt (anionic sodium salt of condensed sulfonic acid) to increase electrical conductivity in order to prevent possible electrostatic problems.

The exact proportions of the mixture were determined experimentally by trial and error. For a trial batch, parameters ρ^* , σ^* , and μ^* were measured at a controlled temperature by means of a hydrometer, a ring type surface tensiometer, and a Cannon-Fenske tube-type viscometer, respectively. The mixture was changed until Eq. (2) was satisfied. Typical values of the fluid properties were $\rho^* = 1.2 \text{ Mg/m}^3$, $\sigma^* = 58 \text{ mN/m}$, and $5 \text{ mPa} \cdot \text{s} \leq \mu^* \leq 20 \text{ mPa} \cdot \text{s}$. Because the water in the mixture evaporated and the glycerol did not, the properties of the mixture changed with time; thus the fluid required regular additions of water.

Modeling apparatus

The apparatus specially constructed for this investigation provides a means of producing a liquid jet, impressing a disturbance upon that jet, viewing the jet breakup process, and measuring the pertinent variables involved.

The water-glycerol model fluid recirculates through the system. The fluid is pumped from a collection tank through a heating coil to maintain a constant temperature and to avoid variation of physical properties due to temperature changes. The fluid then passes through a check valve into a supply tank mounted at the top of the apparatus. A float switch in the tank switches the pump on and off to maintain the fluid level constant within 5 mm (0.2 in.), because a variation in fluid level would cause jet velocity to vary. The fluid, forced by regulated air pressure admitted to the tank, then enters the head, a cylindrical chamber having a bottom plate to which the orifice is attached. The fluid exits through the orifice, forming a liquid jet that is directed vertically downward into the collection funnel and another tank. The orifice is machined into a brass plate that is detachable from the bottom plate of the head, facilitating changes in orifice size or geometry.

A velocity disturbance is impressed on the jet by producing pressure perturbations within the head with a metal bellows that is vibrated vertically by means of a voice-coil actuator. The amplitude and waveform of the disturbance are controlled by the current signal applied to the actuator. Efficient conversion of bellows displacement to perturbation pressure requires that the compliance of the fluid in the head be minimized. Because the presence of air bubbles in the head would increase this compliance, a release valve is located on top of the head to permit the purging of bubbles. To further increase drive efficiency, the fluid enters the head through

JANUARY 1977 INK JET SCALE MODEL

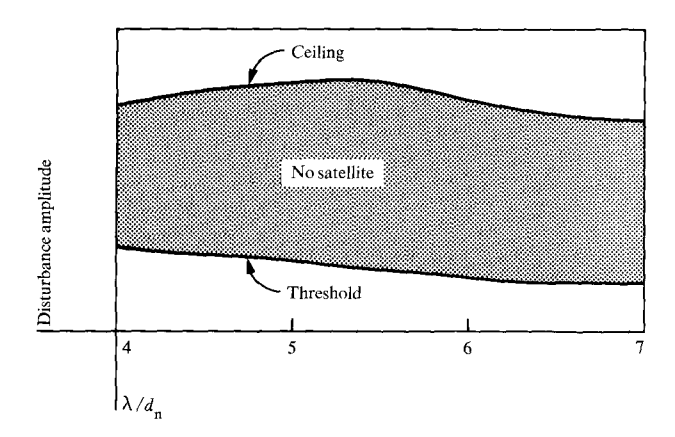


Figure 3 Print window.

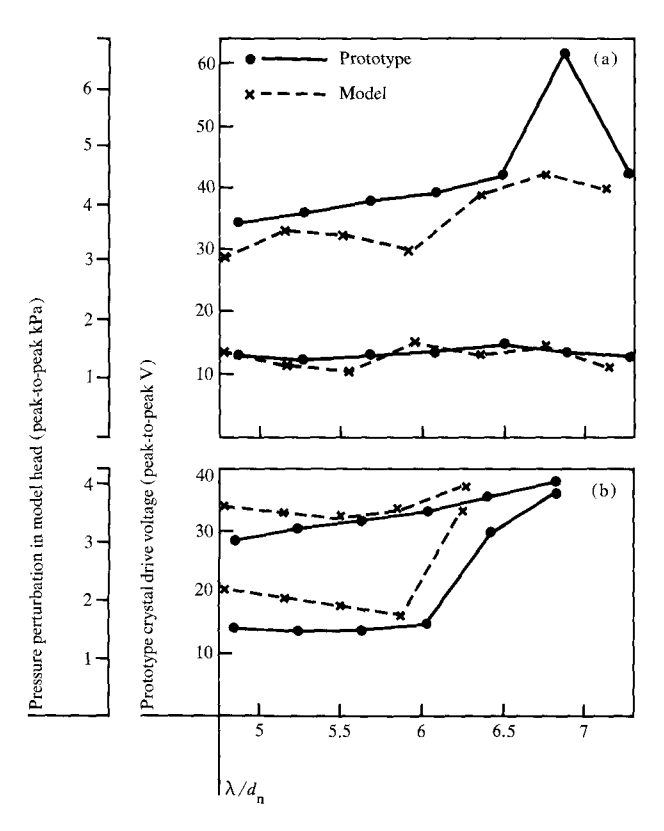


Figure 4 Comparison of model and prototype print windows at operating condition 1: (a) orifice A, (b) orifice B.

a restrictive orifice, without which vibration of the bellows would drive fluid in and out of the head entrance but would produce little perturbational pressure.

A strobe light with a ground glass face is located directly behind the jet. Progress of the drop formation process can be continuously monitored by varying the phase between the disturbance and the strobe flash.

The modeling apparatus is instrumented to measure pertinent variables during a test. A Bourdon pressure gauge and a piezoelectric pressure transducer measure the mean and the perturbation pressures, respectively, at the base of the head near the orifice. Another Bourdon pressure gauge monitors the pressure in the supply tank. A transparent scale mounted alongside the stream measures drop-to-drop separation and breakup distance from the nozzle. The fluid temperature is measured with a mercury thermometer in the collection tank, and the disturbance frequency is displayed on a digital frequency counter.

Ink jet "print point" evaluation

A "print point" is defined by specifying all those jet characteristics that can be considered constant in a given printer design. In the present printer, the print point was defined by giving d_n , l_n , f, ink composition, and excitation waveform within certain tolerances.

The amplitude of the stream excitation signal (which creates \tilde{p} and \tilde{v}) can be varied by printer service personnel. Once this value has been set, the machine is expected to operate properly for an indefinite length of time.

Parameters that may exhibit variations during printer operation due to, for example, variations in temperature are μ , ρ , σ , \bar{p} , \bar{v} , λ , d_i , z_h .

Here μ varies significantly with ink temperature and concentration (i.e., as water evaporates from the recirculating ink); σ and ρ change little. The printer includes a servo system that maintains drop deflection sensitivity by changing ink supply pressure \bar{p} [14], which also causes variations in \bar{v} , λ , d_j , and z_b . An acceptable print point is one that, throughout all the expected variation of parameters μ through z_b , produces drops without satellites.

The primary tool for analyzing a print point is a "velocity print window" (see Fig. 3). It shows the area in the λ/d_n versus disturbance amplitude plane in which no satellites occur. Print windows must be obtained at a number of different ink temperatures and concentrations. A range of disturbance amplitudes and a range of λ/d_n must exist common to each print window. Printer requirements dictate that the "net" print window obtained from this superposition include approximately $4 \le \lambda/d_n \le 7$.

In the model the amplitude of the pressure perturbation in the head serves as the "disturbance amplitude." No means has so far been developed for conveniently measuring the pressure perturbation in the prototype head or for accurately computing it from the piezoelectric crystal energization waveform. Therefore, the voltage amplitude of the signal driving the prototype crystal is considered to be its "disturbance amplitude." A correspondence between model and prototype disturbance

Table 2 Nominal parameter values for two operating conditions.

	Operating condition 1		Operating condition 2	
Parameter	Prototype	Model	Prototype	Model
Perturbation frequency, f (Hz)	104 167	247	117 187	319
Perturbation waveform	sinusoidal	sinusoidal	sinusoidal	sinusoidal
Orifice diameter, d_n (μ m)	32.00	1600	35.05	1600
Orifice aspect ratio, l_n/d_n	1.0	1.0	1.0	1.0
Fluid surface tension, $\sigma''(mN/m)$	72.5	58.0	72.5	58.0
Fluid viscosity, μ (mPa · s)	1.88	12.67	1.88	12.14
Fluid density, ρ (Mg/m ³)	1.037	1.18	1.037	1.18
Modified Weber number, We	5.08	5.08	8.46	8.46
Modified Reynolds number, Re	58.9	58.9	79.4	79.4
Scale factor, K	1.0	50.0	1.0	45.65

Table 3 Dimensions of orifices A and B.

	Orifice A		Orifice B		
	Prototype	Model	Prototype	Model	
Length, l_n (μ m)	28.0	1450	48.0	2510	
Diameter, d_n (μ m)	31.4	1600	31.6	1730	
Aspect ratio, l_n/d_n	0.892	0.906	1.52	1.45	
Entrance radius, $r_{\rm en}$ (μ m)	6.9	292	14.0	508	
Exit radius, $r_{\rm ex}$ (μm)	6.9	300	13.7	452	
$r_{\rm en}/d_{ m n}$	0.22	0.18	0.44	0.29	
$r_{\rm ex}^{\rm en}/d_{\rm n}^{\rm n}$	0.22	0.19	0.43	0.26	

amplitudes is obtained by observing similarities in the relationship between amplitude and breakup distance z_h .

Model validity

Validity of the model was established by a series of experiments in which model and prototype data were compared at two different print points. Table 2 lists the nominal parameter values for both the prototype and the model at the two operating conditions studied.

In one experiment we compared print windows for the model and the prototype at operating condition 1 using different orifices. Measurements were made of two prototype orifices, A and B (see Table 3), and then model orifice plates were made to simulate them. The prototype orifice diameters were measured from a 1000X scanning electron microscope photograph. The bore lengths were determined by viewing the orifices under a microscope equipped with a micrometer stage. The top and bottom surface planes of the orifices were brought into focus, and the lengths were taken to be the differences in the micrometer readings. The edge contour was the most difficult parameter to measure. When the orifice edge was rounded, a dark ring appeared around the orifice when it was top-lighted. The orifice edge was assumed to be rounded at a constant radius equal to the width of this dark ring. Comparisons of the print windows for the orifices are shown in Fig. 4. To plot the model and prototype print windows on the same graph, an average scaling factor for the disturbance amplitude was calculated from the data relating $z_{\rm b}$ to disturbance amplitude. Both the model and prototype print windows show the same trend with changes in orifice geometry.

Another experiment was conducted at operating condition 2 to compare the jet breakup distance as a function of disturbance amplitude on the model and the prototype. The jet breakup distance was recorded as a function of disturbance amplitude at λ/d_n values of 4.0, 5.0, and 6.0. An average disturbance scaling factor was again calculated from the data to plot breakup distance versus the logarithm of the disturbance amplitude for model and prototype on the same graphs, as shown in Fig. 2. The shapes of the curves are very similar for a given value of $\lambda/d_{\rm n}$. A minimum breakup distance $z_{\rm h}$ occurs for both the model and the prototype. The fact that the linear portions of the curves have essentially the same slope indicates that the growth rate of the disturbance is essentially the same for the model and the prototype; however, for a given λ/d_n , the curves are offset by an almost constant amount with respect to breakup distance (i.e., the dimensionless breakup distance is longer for the prototype). As λ/d_n increases, and thus jet velocity increases, the amount of offset also increases al-

JANUARY 1977 INK JET SCALE MODEL

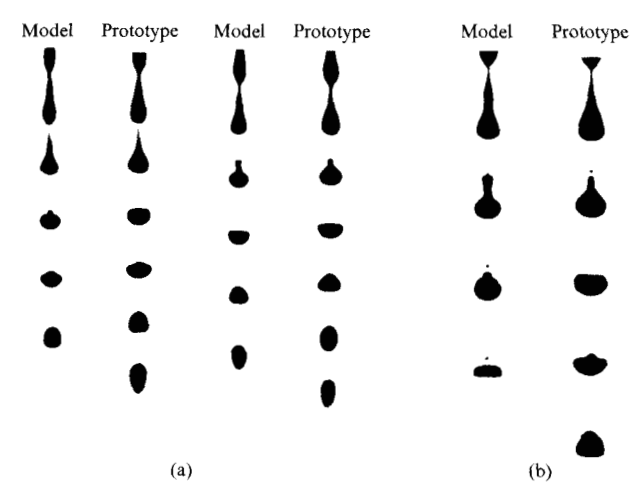


Figure 5 Prototype and model jets at breakup for (a) operating condition 1 and (b) operating condition 2.

most in direct proportion to jet velocity. Thus, based on model data, it appears that the breakup time (z_b/\bar{v}) is approximately 23 μ s longer for the prototype than it should be. A hypothesis to explain this discrepancy (unsupported by any published literature and doubtful in view of what is known about liquid surface tension) is that surface tension takes about 23 μ s to develop and then cause the stream to decay. Another possible explanation is neglect of the Froude number in the modeling.

It is encouraging that the breakup distances for both model and prototype increase with drive amplitude after the decrease predicted by linear theories. At sufficiently high drive amplitudes, this increase has occurred for all streams that we investigated. However, based on intuition and existing analyses of stream breakup, it is unexpected.

Photographs of the model and prototype jets are shown for comparison in Fig. 5. Part of the jet from the nozzle to breakup is not included. The jets are shown at two stages of breakup for operating condition 1. The jet and drop profiles are very similar, and no satellites are formed for this condition. The effect of gravitational acceleration on the model jet is easily seen in the photographs as the model drops overtake the prototype drops. This happens because the model does not simulate the modified Froude number Fr of the prototype. At operating condition 2 a small satellite is formed on both the model and prototype jets. In the case of the prototype the satellite is present for approximately one wavelength and then merges with the drop ahead (forward merging). However, in the model jet, the satellite still exists farther downstream. The satellite forms and moves to contact the drop ahead, just as it does in the prototype jet, but rather than merge with that drop, it rebounds from it. The satellite has formed, moved ahead, and is in contact with the first drop after breakup (as shown in the photograph). This rebounding of satellites did not occur under all model operating conditions, but when it did it was inconsequential because only the presence or absence of satellites mattered. The phenomenon of liquid surfaces touching but not merging has been observed before [15]. Similar to trends shown in [15], we found that an electric field normal to the stream axis prevented the rebounding and allowed the satellite to merge with the drop.

Factors affecting the print window

• Temperature

The scale model proved valuable in evaluating the temperature dependence of the print window. The prototype ink jet printer was designed to operate over a temperature range of 16°C to 38°C.

At one time during printer development, tests conducted on the prototype revealed that as the temperature was decreased from 38°C to 16°C the print window shifted upward so far that the print windows at the two temperatures did not overlap. Thus, no single value of disturbance amplitude could produce a no-satellite condition over that temperature range. Obviously, this temperature dependence would have to be reduced if the printer were to operate over the desired temperature range at a single value of disturbance amplitude. This temperature dependence could be a function of many factors, such as ink viscosity, acoustic velocity in the ink, or damping in the head. The acoustic velocity and the damping may be important because the disturbance amplitude on the prototype is measured in terms of the voltage applied to a piezoelectric crystal diaphragm in the head, rather than in terms of perturbational pressure in the head, as is done on the model. Because the prototype head operates near resonance, a change in the acoustic velocity or damping can significantly modify the transfer function from input voltage to pressure perturbation, which would, in turn, modify the print window.

The scale model was used to separate the effects of fluid viscosity from the other factors and to determine its contribution to the observed change in the print window for the required temperature range. The model was operated at condition 1, and fluid viscosity was varied to simulate ink at 16°C and 38°C. As fluid viscosity was increased to simulate a temperature decrease, the print window shifted upward by 40 percent, much less than the 100 percent observed for the prototype.

The magnitude of this difference suggests that damping in the prototype head was a significant contributing factor to the temperature dependence of the print window. Redesign of a rubber seal around the piezoelectric

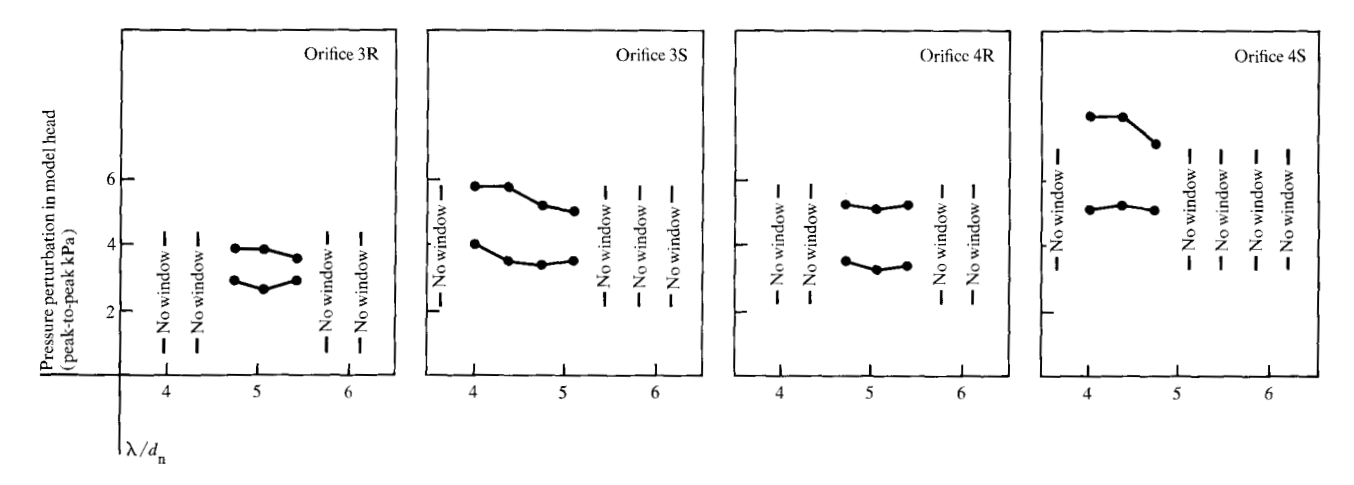


Figure 6 Print windows for various model orifices at operating condition 2.

crystal diaphragm to reduce fluid damping of the crystal in the prototype assembly resulted in a temperature dependence for the prototype that was almost identical to that for the model.

Orifice geometry

The effects of orifice geometry on the print window were studied on the model at operating conditions 1 and 2. Variations in the geometry were limited to changes in $l_{\rm n}/d_{\rm n}$ and to rounded versus sharp entrance and exit edges.

A series of ten orifices having five different $l_{\rm n}/d_{\rm n}$ values with rounded and sharp edges were studied at operating condition 2. Table 4 lists the dimensions of the ten orifices. In general, the print windows obtained with these orifices were unacceptably narrow with respect to disturbance amplitude and extended over only a small range of $\lambda/d_{\rm n}$ values. Some trends were observed, however. The print windows became wider along the amplitude dimension and were shifted upward as $l_{\rm n}/d_{\rm n}$ was increased. Print windows for the sharp-edged orifices occurred at lower $\lambda/d_{\rm n}$ values than those for round orifices. Some of the print windows obtained for this series of orifices are shown in Fig. 6.

Orifice geometry effects were also studied at operating condition 1. The print windows obtained for orifices A and B, discussed previously, give an indication of the orifice geometry effects. Satisfactory print windows were obtained with an $l_{\rm n}/d_{\rm n}$ value of ≈ 1.0 , but higher $l_{\rm n}/d_{\rm n}$ values near 1.5 caused the print window to vanish at the higher $k/d_{\rm n}$ values. Two orifices similar to A and B were made, but with sharp entrance and exit edges. The print windows for these orifices, shown in Fig. 7, indicate that sharp edges are undesirable. Sharp edges on orifice B caused the print window to vanish at

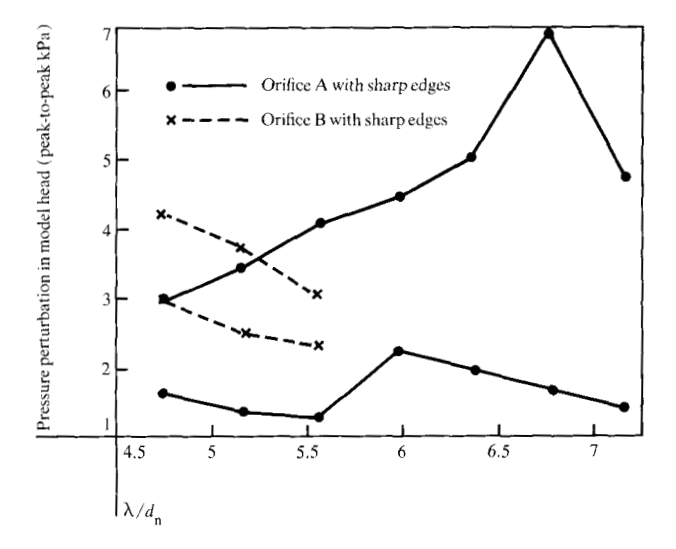


Figure 7 Print windows at operating condition 1 for model orifices similar to orifices A and B but with sharp edges.

Table 4 Dimensions of model orifices used to study orifice geometry effects.

Orifice number	$\binom{l_n^*}{(\mu m)}$	$d_n^* \over (\mu m)$	$I_{\rm n}^*/d_{\rm n}^*$	$rac{r_{ m en}^*}{(\mu{ m m})}$	$r_{\mathrm{ex}}^* (\mu \mathrm{m})$
18	950	1560	0.61	0	0
2S	1590	1570	1.01	0	0
3S	2220	1570	1.41	0	0
4S	2860	1560	1.83	0	0
5S	3490	1550	2.25	0	0
1 R	950	1610	0.59	180-230	180-230
2R	1590	1600	0.99	180-230	180-230
3R	2220	1580	1.41	180-230	180-230
4R	2860	1590	1.80	250	270
5R	3490	1600	2.18	280	330

Table 5 Relative print windows for 25 jet conditions and 3 λ/d_n values.

$\lambda/d_{\rm n}$	We	52.7	61.8	<u>Re</u> 70.9	80.0	89.1
	10.25	1.39	1.44	1.47	1.46	1.33
	8.60	1.49	1.48	1.51	1.58	1.55
4.5	6.95	1.74	1.51	1.63	1.96	1.67
4.5	5.30	1.88	2.14	2.45	1.83	1.74
	3.65	2.43	2.90	2.38	2.62	2.34
	10.25	1.55	1.30	1.28	1.20	1.09
	8.60	2.04	1.34	1.47	1.17	1.17
5.0	6.95	1.72	1.54	1.95	1.38	1.53
	5.30	2.64	3.00	3.25	2.94	1.85
	3.65	3.24	3.30	3.36	3.71	3.00
	10.25	3.10	2.00	NW	NW	NW
	8.60	3.50	1.13	NW	NW	NW
5.5	6.95	2.30	1.75	1.18	1.14	1.18
	5.30	3.73	2.26	2.07	1.88	1.85
	3.65	3.68	2.85	2.57	2.58	2.49

a lower value of λ/d_n , and sharp edges on orifice A caused a rise in the print window threshold at the higher λ/d_n values.

Orifice geometry is important with respect to satellite formation, and it must, therefore, be controlled. However, the effect of orifice geometry on the print window is dependent upon the values of the other parameters that are needed to describe a print point. Thus, a given change in geometry may affect the print window quite markedly at one operating condition but may have little effect at another.

• Print point

During the study of orifice geometry, a marked difference in satellite behavior was observed for two different print points, even when using orifices of similar geometry. Therefore, this difference in satellite behavior must be, in some way, related to the other parameters that describe the operating condition. Because the disturbance used in both tests was sinusoidal, the only parameters that varied from condition 1 to condition 2 were those that describe the properties of the jet itself. We therefore conducted an experiment on the model to investigate the relation between the jet properties and the print window.

The parameters that describe the jet were grouped into two independent dimensionless parameters, the modified Weber number \underline{We} and the modified Reynolds number \underline{Re} . These parameters were particularly useful, because they remain constant as jet velocity is varied to plot the print window.

The relationship between these two dimensionless parameters and the print window was determined by plotting print windows for all combinations of five different \underline{We} and five different \underline{Re} numbers (i.e., 25 different jet conditions). The ranges of \underline{We} and \underline{Re} were chosen such that the jet conditions for operating conditions 1 and 2 were included. A single orifice having an l_n/d_n value of 0.996 and rounded edges was used for all tests.

Definite trends were observed between the values of the dimensionless parameters and the print window. The print windows for the 25 different jet conditions are summarized at λ/d_n values of 4.5, 5.0, and 5.5 in Table 5 showing the ratio of the ceiling disturbance amplitude to the threshold disturbance amplitude (i.e., a relative print window height) for the various jet conditions. An entry of NW means that no window existed. The most obvious conclusion from the table is that the print window improves as We is decreased, regardless of Re. The print window also improves with decreasing Re in some cases, especially at the higher λ/d_n values. The jet properties for operating conditions 1 and 2 correspond very closely to two conditions shown in Table 5. The complete print windows for these conditions are plotted in Fig. 8, showing that a much better print window is obtained with the lower values of We and Re.

The effects of the individual jet parameters on the print window and the relative effectiveness of each can be determined from the definitions of <u>We</u> and <u>Re</u>. Considering the modified Weber number, the print window can be improved by decreasing the density, the perturbation frequency, or the jet diameter or by increasing the surface tension. The relative effectiveness of proportional changes in these parameters is indicated by their exponent in the equation for <u>We</u>. Parameter <u>Re</u> can be reduced by decreasing the density, perturbation frequency, or jet diameter, and also by increasing the viscosity.

Suppose the prototype printer is operating at condition 2 and the print window is to be improved by decreasing We and Re. This can be accomplished by changing several parameters; however, in the case of a printer with fixed drop frequency, drop frequency and jet diameter are basic printer parameters and cannot be changed without affecting machine speed and/or print resolution. This leaves three possible changes in jet properties: Reduce the density, increase the surface tension, or increase the viscosity. All three of these approaches were considered impractical for the prototype because the density of the ink was already very low, the dynamic surface tension was already very high, and an increase in viscosity would cause numerous other problems, such as increased pump pressure requirements and an increased viscosity index. Thus, if the printing scheme was to be achieved on the prototype, relatively high values of We and Re were inevitable and some means of improving the print window other than changing jet properties had to be found.

• Disturbance harmonics

Thus far, the effects on the print window of orifice geometry and jet properties, while maintaining sinusoidal perturbation, have been discussed. Another parameter important to the jet breakup process is the harmonic content of the impressed disturbance. The effect of mixing the second harmonic with the disturbance fundamental was investigated at operating condition 2. A marked improvement in the print window resulted when the relationship between the fundamental and the harmonic was at the proper phase and amplitude. The resulting perturbation pressure in the model head had a triangular waveform with a slow rise and fast decline. Mixing the second harmonic was also beneficial on the prototype. The required relationship between the fundamental and the second harmonic is present in a biased square wave that is 40 percent up and 60 percent down. Although this waveform contains many higher harmonics, it produced nearly the same effect as mixing only the second harmonic. Print windows for the prototype at condition 2 with and without harmonic mixing are shown in Fig. 9.

Conclusion

A scale ink jet model was used to study the relation between the occurrence of satellite drops and several parameters. The effect of orifice geometry was found to be largely dependent on the values of the other parameters. The parameters that describe the jet itself were grouped into two independent dimensionless parameters, and definite trends were observed between the values of these parameters and the occurrence of satellites. The harmonic content of the impressed disturbance was found to markedly affect the occurrence of satellites at one of the operating conditions. It is emphasized that the trends and relationships observed pertain to a limited range of operating conditions and may not be valid over some other range of conditions.

The model was very useful for its intended purpose of helping us to understand the parameters affecting satellite formation. It provided an early indication of the occurrence of very small satellites (Fig. 5b), which until that time had not been observed on the prototype. Consequently, the prototype strobe flash duration was decreased and the existence of these satellites confirmed. These small satellites appear to be of a different type from those commonly found and mentioned in [9] because they do not contain most of the fluid of the ligament that exists between drops shortly before breakup. Instead they contain only a very small portion from the pointed rear end of the filament.

The shape of the curve of breakup distance versus drive amplitude was modeled well except for an offset in the z_b direction; the breakup distance on the model was consistently shorter than on the prototype. This differ-

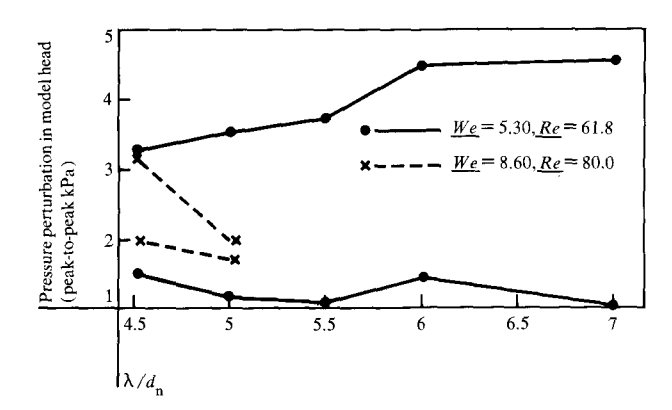


Figure 8 Effect of jet parameters on print window.

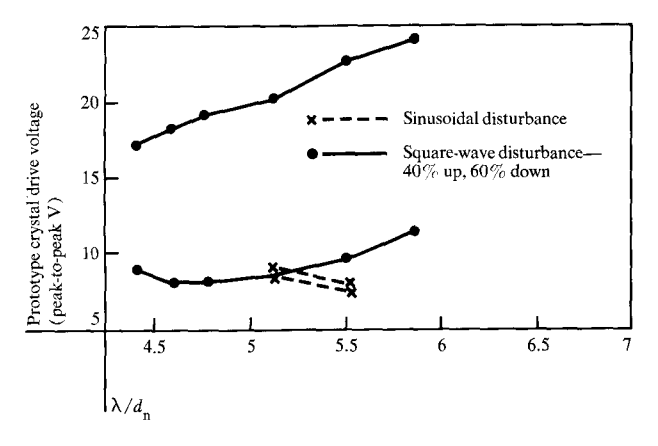


Figure 9 Effect of disturbance harmonics; conditions are the same as operating condition 2 except that $\mu = 1.42$ mPa·s.

ence may imply an unsuspected transient behavior of the surface tension of a stream leaving a nozzle; it may be due to not having modeled the Froude number; or it may be due to some other unsuspected phenomenon.

Our experience with the model indicates that experiments on the model and prototype must be pursued simultaneously and results compared. When the behavior of the two is the same, one is confident of getting valid data. When the behavior is different in an important way, one must investigate the possible causes of the discrepancy. Changes in either the model or the prototype may be called for.

Acknowledgments

The model hardware was designed and its assembly coordinated by R. E. Bishop, IBM Office Products Division, Boulder. Throughout our experimentation this model proved itself reliable in operation and adaptable to the desired test conditions. Professor R. Eichhorn, Dept. of Mechanical Engineering, University of Kentucky, first proposed the study of synchronous drop formation using a scale model. He designed and experimented with a forerunner of the present model.

Appendix: Glossary

value, mean value, and perturbation of pres-
sure at the nozzle entrance
value, mean value, and perturbation of jet
velocity, respectively
nozzle diameter
nozzle length
jet diameter
breakup distance
drop-to-drop spacing
drop frequency
density
surface tension
dynamic viscosity
modified Weber number, $\rho f^2 d_n^3 / \sigma$
modified Reynolds number, $\rho f d_n^2 / \mu$
modified Froude number, $f\sqrt{d_{\rm n}/g}$
modified Strouhal number, $\bar{v}_i/f\lambda$
pressure coefficient, $\bar{p}/\rho \bar{v}_{j}^{2}$

References

- F. Savart, "Mémoire sur la Constitution des Veines Liquides Lancées par des Orifices Circulaires en Mince Paroi," Annales de Chimie et de Physique 53, 337 (1833).
- G. Magnus, "Hydraulische Untersuchungen; Ueber die Bäuche der Strahlen aus Kreisförmigen Oeffnungen," Poggendorff's Annal 106, 1 (1859).
- 3. J. W. S. Rayleigh, "On the Instability of Jets," Proc. London Math. Soc. 10, 4 (1878).

- 4. W. L. Buehner, J. D. Hill, T. H. Williams, and J. W. Woods, "Application of Ink Jet Technology to a Word Processing Output Printer," *IBM J. Res. Develop.* 21, 2 (1977, this issue).
- G. L. Fillmore, W. L. Buehner, and D. L. West, "Drop Charging and Deflection in an Electrostatic Ink Jet Printer," IBM J. Res. Develop. 21, 37 (1977, this issue).
- J. W. S. Rayleigh, "On the Capillary Phenomena of Jets," Proc. Roy. Soc. Sec. A, Math. Phys. Sci. 29, 71 (1879).
- H. C. Lee, "Drop Formation in a Liquid Jet," IBM J. Res. Develop. 18, 364 (1974).
- 8. M. C. Yuen, "Non-linear Capillary Instability of a Liquid Jet." J. Fluid Mech. 33, 151 (1968).
- 9. W. T. Pimbley and H. C. Lee, "Satellite Droplet Formation in a Liquid Jet," *IBM J. Res. Develop.* 21, 21 (1977, this issue).
- L. Crane, S. Birch, and P. D. McCormack, "An Experimental and Theoretical Analysis of Cylindrical Jets Subjected to Vibration," *Brit. J. Appl. Phys.* 16, 395 (1965).
- J. M. Schneider, H. R. Lindblad, C. D. Hendricks, Jr., and J. M. Crowley, "Stability of an Electrified Liquid Jet," J. Appl. Phys. 38, 2599 (1967).
- G. Murphy, Similitude in Engineering, The Ronald Press Company, New York 1950.
- W. N. Bond and H. O. Puls, "The Change of Surface Tension with Time," *Phil. Mag.* (Supplement) 24, 864 (1937).
- J. M. Carmichael, "Controlling Print Height in an Ink Jet Printer," IBM J. Res. Develop. 21, 52 (1977, this issue).
- C. L. Stong, "The Amateur Scientist," Sci. Am. 229, 104 (1973).

Received April 1, 1976; revised August 16, 1976

The authors are located at the IBM Office Products Division laboratory, Lexington, KY 40507.